PNAS RESEARCH ARTICLE | NEUROSCIENCE OPEN ACCESS

Astrocytic EphA4 signaling is important for the elimination of excitatory synapses in Alzheimer's disease

Xin Yang[a,b], Ye Wang[a], Yi Qiao[a,b], Jingwen Lin[a], Jackie K. Y. Lau[a,b], Wing-Yu Fu[a,b], Amy K. Y. Fu[a,b,c], and Nancy Y. Ip[a,b,c,1]

Affiliations are included on p. 10.

Contributed by Nancy Y. Ip; received October 3, 2024; accepted December 10, 2024; reviewed by Evandro F. Fang and Lin Mei

Cell surface receptors, including erythropoietin-producing hepatocellular A4 (EphA4), are important in regulating hippocampal synapse loss, which is the key driver of memory decline in Alzheimer's disease (AD). However, the cell-specific roles and mechanisms of EphA4 are unclear. Here, we show that EphA4 expression is elevated in hippocampal CA1 astrocytes in AD conditions. Specific knockout of astrocytic EphA4 ameliorates excitatory synapse loss in the hippocampus in AD transgenic mouse models. Single-nucleus RNA sequencing analysis revealed that EphA4 inhibition specifically decreases a reactive astrocyte subpopulation with enriched complement signaling, which is associated with synapse elimination by astrocytes in AD. Importantly, astrocytic EphA4 knockout in an AD transgenic mouse model decreases complement tagging on excitatory synapses and excitatory synapses within astrocytes. These findings suggest an important role of EphA4 in the astrocyte-mediated elimination of excitatory synapses in AD and highlight the crucial role of astrocytes in hippocampal synapse maintenance in AD.

Alzheimer's disease | Eph receptors | synapse loss | reactive astrocytes | complement signaling

Significance

Cognitive impairment in Alzheimer's disease (AD) is largely attributed to hippocampal synapse loss. Importantly, astrocytes are the primary glial cells whose malfunction results in excitatory synapse elimination in AD. However, the cellular mechanisms in this process remain unclear. Here, we show that astrocyte-specific deletion of erythropoietin-producing hepatocellular A4 (EphA4) restores excitatory synapse loss in AD transgenic mouse models. Multiomics analysis of the mouse hippocampus shows that EphA4 inhibition increases synaptic components and decreases reactive astrocytes. Importantly, knockout of astrocytic but not neuronal EphA4 decreases astrocyte reactivity, complement signaling activation, and astrocytic engulfment of excitatory synapses in the hippocampus in AD. In summary, astrocytic EphA4 is an important cellular signaling that regulates hippocampal synapse loss and synaptic dysfunction in AD.

Alzheimer's disease (AD) is a progressive neurological disorder characterized by a gradual decline in cognitive functions, particularly memory. Early pathological changes in the hippocampus, including synaptic disruption and dysfunction, are key contributors to memory deficits (1, 2). The entorhinal–hippocampal circuit is one of the first affected circuits in AD. The hippocampus is particularly vulnerable to synaptic damage and synapse loss in the early stage of AD (3–5). Within the hippocampus, the Schaffer collateral (SC) pathway, which connects cornu ammonis 3 (CA3) and CA1 pyramidal neurons, plays a vital role in spatial and contextual memory consolidation and retrieval (6–8). However, the integrity of this hippocampal circuitry is compromised in AD (9, 10). This leads to impaired neurotransmitter release and diminished synaptic plasticity, which contribute to the memory impairment observed in individuals with AD.

Meanwhile, the accumulation of neurotoxic amyloid-beta (Aβ) oligomers in the hippocampus induces both the impairment of synaptic transmission and loss of excitatory synapses during AD progression. These Aβ oligomers impair excitatory synaptic transmission via the disruption of presynaptic neurotransmitter release and synaptic vesicle dynamics (11, 12) as well as the degradation of glutamate receptors (13–18). Meanwhile, excitatory synapse loss is due to the neurotoxicity of bound Aβ oligomers and the subsequent induction of neuronal and glial dysfunction (19). Consequently, the compromised synaptic transmission and reduction of synapses induced by soluble Aβ oligomers lead to impaired synaptic plasticity, resulting in desynchronized network activity (20, 21).

Hippocampal synapse loss in AD is largely attributable to glial cell dysfunction, particularly the elimination of excitatory and inhibitory synapses by astrocytes and microglia (22–25). In AD, the elimination of excitatory synapses is mainly mediated by astrocytes in the hippocampus (24, 26, 27). Astrocytes have recently been implicated for their role in maintaining excitatory–inhibitory synapse homeostasis by eliminating redundant synapses through phagocytic receptors (e.g., Megf10 and Mertk) (28, 29). These receptors are activated by the signals that stimulate phagocytosis (e.g., phosphatidylserine and complements) (30, 31). In brain injury, aging, or neurodegenerative diseases including AD, astrocytes become hyperactive and excessively engulf synapses, thereby contributing to synapse loss. The synapse elimination activity of astrocytes in AD is induced via their interaction with C1q, an innate immune protein that is an initiator of the classical complement cascade at synapses (24). C1q induces astrocyte reactivity, leading to the release of C3; therefore, astrocyte hyperreactivity is associated with increased synapse engulfment (27). However, the molecular mechanisms of C1q-induced synapse elimination in astrocytes in AD remain unclear.

Reviewers: E.F.F., Universitetet i Oslo; and L.M., Chinese Institutes for Medical Research.

The authors declare no competing interest.

[1]To whom correspondence may be addressed. Email: boip@ust.hk.

This article contains supporting information online at https://www.pnas.org/lookup/suppl/doi:10.1073/pnas.2420324122/-/DCSupplemental.

Published February 10, 2025.

In AD, Aβ triggers the cell-type-specific regulation of synapse loss through the activation of specific cell surface receptors (19, 32–34). One candidate receptor involved in this mechanism is erythropoietin-producing hepatocellular A4 (EphA4) (35), a member of the erythropoietin-producing hepatocellular (Eph) receptor family that is expressed in both neurons and astrocytes in the brain. EphA4 maintains hippocampal synaptic plasticity by regulating structural synaptic plasticity and the levels of AMPA receptors (36–38). A genome-wide association study suggests that a single-nucleotide polymorphism located at the 3′-untranslated region of the *EPHA4* gene is associated with AD risk (39). While the activity of EphA4 is elevated in the hippocampus in AD mouse models (35, 37), blockade of EphA4 signaling ameliorates the decrease of excitatory synapses in cultured hippocampal neurons induced by soluble Aβ and alleviates impaired synaptic plasticity in an early-aged AD mouse model (35). Moreover, EphA4 expression is associated with astrogliosis response, particularly upon ischemic insult or nerve injury (40–42). Nevertheless, the cell-type-specific roles of EphA4, particularly in astrocytes, in synaptic impairment in AD and its underlying cellular and molecular mechanisms remain largely unclear.

Therefore, in this study, we investigated the roles of astrocytic EphA4 signaling in the regulation of hippocampal excitatory synaptic structure and functions in AD using transgenic mouse models, including APP/PS1 and 5XFAD mice. We found that EphA4 expression was up-regulated in the hippocampal CA1 pyramidal neurons and astrocytes of these AD mouse models. Meanwhile, genetic deletion of EphA4 in astrocytes rescued synapse loss and dendritic spine alterations in AD transgenic mice. Single-nucleus RNA sequencing (snRNA-seq) analysis revealed that EphA4 inhibition restored synapse-related gene expression in hippocampal CA3 and CA1 neurons while decreasing astrocyte stress and reactivity in AD transgenic mice. Furthermore, specific knockout of EphA4 in astrocytes in AD transgenic mice decreased astrocyte hyperreactivity, the tagging of excitatory synapses by a complement protein, and the engulfment of excitatory synapses by astrocytes. Thus, our findings reveal the distinct role of astrocytic EphA4 in synaptic dysfunction, highlighting a dysregulated mechanism of astrocytes in synaptic dysfunction in AD.

Results

EphA4 Expression Is Elevated in Hippocampal CA1 Neurons and Astrocytes in Alzheimer's Disease. To elucidate the cell-specific roles of the EphA4 receptor in AD-associated hippocampal synaptic dysfunction, we examined the regulation of EphA4 expression in the hippocampus in APP/PS1 mice, a well-established transgenic mouse model of AD. In 6-mo-old wild-type (WT) mice, EphA4 expression was predominantly observed in pyramidal neurons within the hippocampal CA1 region and remained relatively unchanged upon aging (Fig. 1 *A*–*C*). In contrast, we observed notably greater EphA4 expression in the CA1 pyramidal neurons of 12-mo-old APP/PS1 mice than in age-matched WT controls (Fig. 1 *A*–*C*). This elevated EphA4 expression was specific to CA1 pyramidal neurons; we detected no significant changes in CA3 pyramidal neurons (*SI Appendix*, Fig. S1 *A* and *C*).

Approximately 40% of hippocampal CA1 astrocytes in WT mice of various ages expressed EphA4. However, in APP/PS1 mice, the proportion of *Epha4*$^+$ astrocytes in the hippocampal CA1 region was significantly greater than that in the WT controls at corresponding ages (Fig. 1 *D*–*F*); this effect was not apparent in the CA3 region (Fig. 1 *D*–*F*). We also observed a similar pattern of elevated *Epha4* transcript levels in pyramidal neurons and a greater proportion of *Epha4*$^+$ astrocytes in the CA1 region in 9-mo-old 5XFAD mice, another AD transgenic mouse model (*SI Appendix*, Fig. S2). Together, these findings indicate specific cellular dysregulation of EphA4 in the hippocampal CA1 region

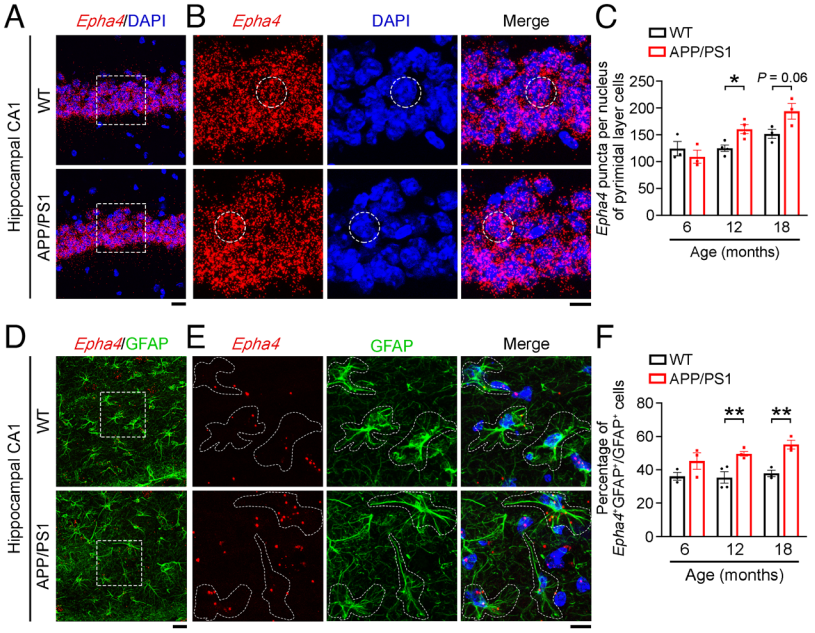

Fig. 1. EphA4 expression is elevated in hippocampal CA1 pyramidal neurons and astrocytes in APP/PS1 mice. (*A*–*F*) Developmental expression of EphA4 in hippocampal CA1 pyramidal cells (*A*–*C*) and astrocytes (*D*–*F*) in 6-, 12-, and 18-mo-old APP/PS1 and WT mice. (*A*) Representative images of in situ hybridization (i.e., RNAscope) showing the expression of *Epha4* in the hippocampal CA1 pyramidal layer in 12-mo-old APP/PS1 and WT mice. (Scale bar: 20 μm.) White dashed boxes outline areas of high magnification shown to the *Right*. (*B*) Representative zoomed-in images. (Scale bar: 10 μm.) White dashed circles indicate nuclei with average *Epha4* puncta. (*C*) Quantitative analysis of *Epha4* puncta per nucleus in the pyramidal cell layer (n = 3, 4, and 3 mice aged 6, 12, and 18 mo, respectively; *P < 0.05; unpaired two-tailed Student's t test). (*D*) Representative RNAscope images showing *Epha4* expression in hippocampal CA1 astrocytes in 12-mo-old APP/PS1 and WT mice. (Scale bar: 20 μm.) White dashed boxes outline areas of high magnification shown to the *Right*. (*E*) Representative zoomed-in images. (Scale bar: 10 μm.) White dashed outlines indicate astrocytes with average *Epha4* puncta. (*F*) Quantitative analysis of the percentage of *Epha4*$^+$ astrocytes (n = 3, 4, and 3 mice aged 6, 12, and 18 mo, respectively; **P < 0.01; unpaired two-tailed Student's t test). Data are mean ± SEM.

in AD transgenic mice, implicating it in the synaptic dysfunctions characteristic of AD.

CA1 Neuronal and Astrocytic EphA4 Play Critical Roles in Excitatory Synapse Loss in Alzheimer's Disease. In our previous study, blockade of EphA4 activity abolished synapse loss in hippocampal neurons induced by synaptotoxic oligomeric Aβ and ameliorated impairments in hippocampal synaptic plasticity in an AD transgenic mouse model (35). Building on this foundation, in the current study, we dissected the distinct roles of neuronal and astrocytic EphA4 in the functional dysregulation of hippocampal SC–CA1 synapses in AD. Accordingly, we employed a genetic approach to specifically knock out EphA4 in either neurons or astrocytes within the CA1 region of APP/PS1 × EphA4$^{lx/lx}$ mice (*SI Appendix*, Figs. S3 and S4).

While APP/PS1 mice exhibited a significant decrease of excitatory synapses upon EphA4 knockout, as indicated by decreased colocalization of presynaptic VGluT1 and postsynaptic PSD-95 (Fig. 2 *A*–*C*), EphA4 knockout in the CA1 neurons of APP/PS1 mice restored the density of excitatory synapses to a level comparable to that in WT mice (Fig. 2 *A*–*D*). This finding demonstrates that deletion of postsynaptic hippocampal neuronal EphA4 rescues synapse loss in AD. Interestingly, knockout of astrocytic EphA4 in the hippocampal CA1 region in APP/PS1 mice also resulted in increased excitatory synapse density (Fig. 2 *A*–*D*), indicating that astrocytic EphA4 has a specific role in mediating hippocampal synapse loss in AD.

Most excitatory synapses are on dendritic spines, and abnormalities in their morphology and density are associated with synaptic dysfunction. Compared to APP/PS1 transgenic mice, knockout of either neuronal or astrocytic EphA4 in the hippocampal CA1 region in APP/PS1 mice led to an increase in total dendritic spine density, particularly the number of mature spines (Fig. 2 *E*–*H*). Notably, only neuronal EphA4 knockout resulted in a reduction in immature spines in the CA1 neurons of APP/PS1 mice; astrocytic EphA4 knockout did not affect the number of immature spines (Fig. 2 *E* and *H*). These findings suggest that neuronal and astrocytic EphA4 have distinct regulatory roles in shaping dendritic spine morphology. In addition, we observed similar increases in the numbers of excitatory synapses and dendritic spines following CA1 neuronal or astrocytic EphA4 knockout in 5XFAD mice (*SI Appendix*, Fig. S5). Together, these results highlight the distinct, critical contributions of neuronal and astrocytic EphA4 signaling to synaptic maintenance and dendritic spine morphogenesis in the hippocampus during AD progression.

EphA4 Inhibition Rescues Excitatory Synapse Loss and Alleviates Hippocampal Synaptic Dysfunctions in Alzheimer's Disease. To examine the effects of EphA4 inhibition on hippocampal synaptic functions in AD, we treated APP/PS1 mice with KYL peptide, a

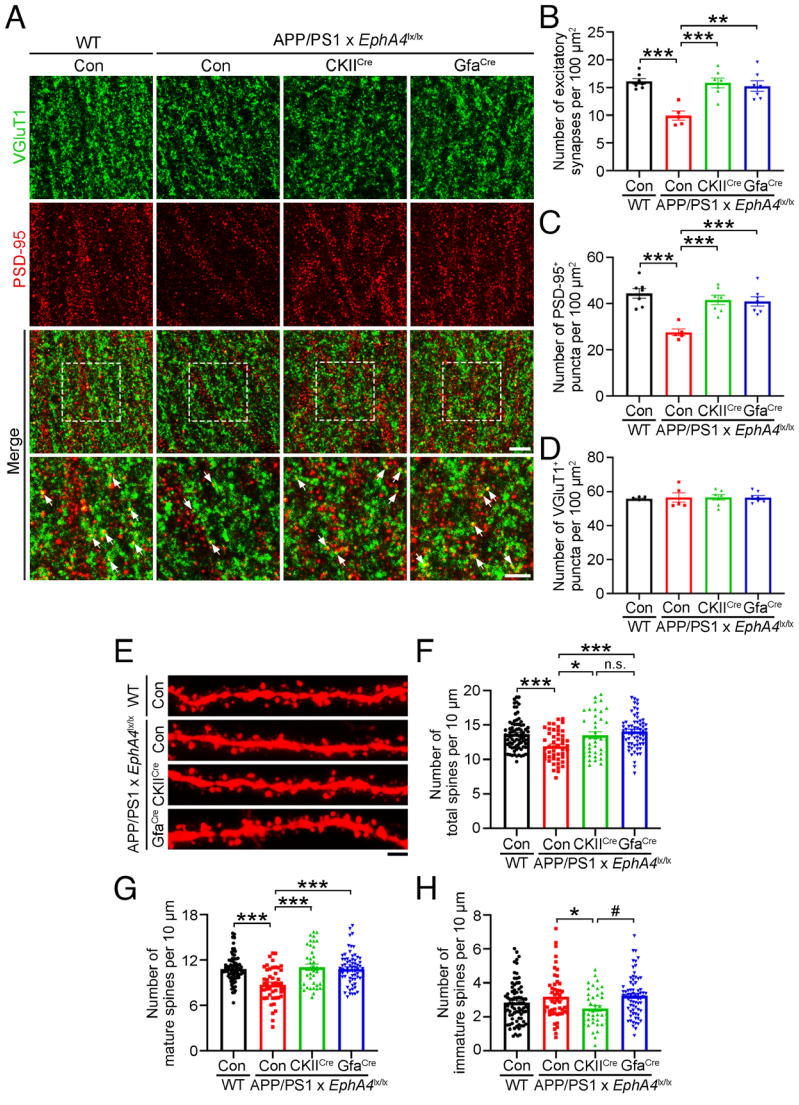

Fig. 2. Deletion of CA1 astrocytic EphA4 restores the excitatory synapse loss in APP/PS1 mice. (*A*–*D*) Immunohistochemical analysis of PSD-95 and VGluT1 in the hippocampal CA1 region of 12-mo-old APP/PS1 × EphA4$^{lx/lx}$ mice after conditional knockout of neuronal or astrocytic EphA4 in the hippocampal CA1 region. (*A*) Representative images, including overlay images and higher-magnification segmented images, showing PSD-95 and VGluT1 clusters (*Top* and *Bottom* scale bars: 5 and 2 μm, respectively). White dashed boxes outline areas of high magnification shown on the *Bottom*. White arrows indicate VGluT1$^+$ PSD-95 clusters. (*B*–*D*) Quantification of excitatory synapses (*B*), postsynaptic PSD-95$^+$ puncta (*C*), and presynaptic VGluT1$^+$ puncta (*D*) (wild-type [WT] × EphA4$^{lx/lx}$ AAV9-CaMKIIa [Con]: $n = 7$ mice, APP/PS1 × EphA4$^{lx/lx}$ Con: $n = 5$ mice, APP/PS1 × EphA4$^{lx/lx}$ AAV9-CaMKIIa-Cre [CKII^{Cre}]: $n = 7$ mice, APP/PS1 × EphA4$^{lx/lx}$ AAV9-GfaABC1D-Cre [Gfa^{Cre}] virus injection: $n = 7$ mice; one-way ANOVA followed by post hoc Tukey's test). (*E*–*H*) Structural modifications of dendrites after conditional knockout of neuronal or astrocytic EphA4 in the hippocampal CA1 region of 12-mo-old APP/PS1 × EphA4$^{lx/lx}$ mice. (*E*) Representative images showing dendritic spine morphology labeled with mCherry. (Scale bar: 2 μm.) (*F*–*H*) Quantification of total spine density (*F*), mature spine density (*G*), and immature spine density (*H*) (WT × EphA4$^{lx/lx}$ Con: $n = 79$ dendrites from 7 mice, APP/PS1 × EphA4$^{lx/lx}$ Con: $n = 48$ dendrites from 4 mice, APP/PS1 × EphA4$^{lx/lx}$ CKII^{Cre}: $n = 40$ dendrites from 4 mice, APP/PS1 × EphA4$^{lx/lx}$ Gfa^{Cre}: $n = 69$ dendrites from 6 mice; $^*P < 0.05$, $^{**}P < 0.01$, $^{***}P < 0.001$, and $^{\#}P < 0.05$; one-way ANOVA followed by post hoc Tukey's test). Data are mean ± SEM.

specific EphA4 inhibitor (35) (Fig. 3*A*). In the hippocampal CA1 neurons of APP/PS1 mice, KYL treatment led to more excitatory synapses and postsynaptic PSD-95 puncta (Fig. 3 *B*–*E*) as well as higher densities of total and mature dendritic spines (Fig. 3 *F*–*I*). Furthermore, KYL treatment led to the restoration of synaptic transmission at SC–CA1 synapses in APP/PS1 transgenic mice. In response to increasing stimulus current, APP/PS1 control mice exhibited notably lower fiber volley (FV) amplitude, which is a measure of the number of firing action potentials in CA3 neurons, and a lower slope of field excitatory postsynaptic potentials (fEPSPs), which reflects basal synaptic transmission (Fig. 3 *J* and *K*). However, KYL treatment in APP/PS1 mice led to the restoration of FV amplitude and a trend toward increased fEPSP slope (Fig. 3 *J* and *K*), indicating that blockade of EphA4 signaling increases the strength of synaptic connections in AD conditions.

The restoration of synaptic transmission in KYL-treated APP/PS1 mice was also accompanied by amelioration of decreased hippocampal synaptic plasticity, specifically long-term potentiation (LTP) in the SC–CA1 pathway, which was observed in APP/PS1 control mice (Fig. 3 *L* and *M*). Together, these results indicate that EphA4 inhibition not only restores the loss of excitatory synapses but also ameliorates the impaired synaptic functions in AD.

EphA4 Inhibition Restores Molecular Phenotypes Associated with Synaptic Functions in the Hippocampus in Alzheimer's Disease. To examine the effects of EphA4 inhibition on the cellular and molecular phenotypes within the SC pathway in AD, we performed snRNA-seq analysis on hippocampal tissues from KYL-treated APP/PS1 mice (Fig. 4*A* and *SI Appendix*, Fig. S6*A*). We clustered the hippocampal nuclei according to their gene expression profiles (*SI Appendix*, Fig. S6*B* and Dataset S1) and determined cell identities according to established datasets (43, 44). The identified cell types included dentate gyrus granule cells, CA3 excitatory neurons, CA1 excitatory neurons, subiculum excitatory neurons, inhibitory neurons, astrocytes, microglia, endothelial cells, oligodendrocyte progenitor cells, epithelial cells, and fibroblasts (Fig. 4*A*). The proportions of the nuclei of each cell type remained consistent across the KYL-treated APP/PS1 mice, APP/PS1 control mice, and WT control mice (*SI Appendix*, Fig. S6*C*).

We subsequently compared the transcriptome profiles of hippocampal CA3 and CA1 excitatory neurons under different conditions (Dataset S2). Gene Ontology (GO) analysis revealed that compared to the WT control mice, the differentially expressed genes (DEGs) up-regulated in the APP/PS1 control mice were enriched in pathways related to oxidative stress, apoptosis, and cytoskeleton organization (blue clusters in Fig. 4 *B*–*E*). The expression levels of these DEGs in the KYL-treated APP/PS1 mice

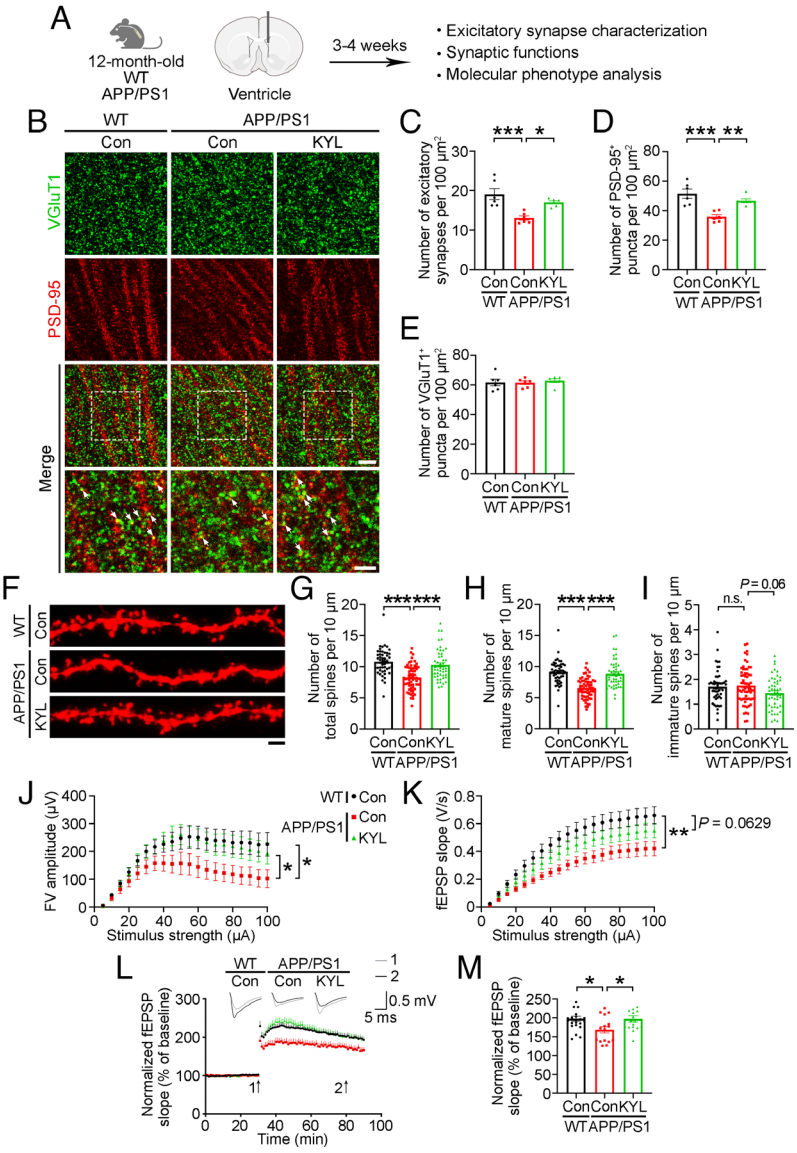

Fig. 3. Blockade of EphA4 signaling rescues the loss of excitatory synapses and impairment of hippocampal synaptic transmission in APP/PS1 mice. (*A*) Schematic diagram of experimental design and analysis. (*B*–*E*) Immunohistochemical analysis of PSD-95 and VGluT1 in the hippocampal CA1 region of 12-mo-old APP/PS1 mice after KYL treatment. (*B*) Overlay and zoomed-in images showing PSD-95 and VGluT1 clusters (*Top* and *Bottom* scale bars: 5 and 2 μm, respectively). White dashed boxes outline areas of high magnification shown on the *Bottom*. White arrows indicate VGluT1$^+$ PSD-95 clusters. (*C*–*E*) Quantification of excitatory synapses (*C*), postsynaptic PSD-95$^+$ puncta (*D*), and presynaptic VGluT1$^+$ puncta (*E*) (n = 6 mice per group; ***P < 0.001 and **P < 0.01; one-way ANOVA followed by post hoc Tukey's test). (*F*–*I*) Structural modifications of dendrites in the hippocampal CA1 region of 12-mo-old APP/PS1 mice after KYL treatment. (*F*) Representative images showing dendritic spine morphology labeled with mCherry. (Scale bar: 2 μm.) (*G*–*I*) Quantification of total spine density (*G*), mature spine density (*H*), and immature spine density (*I*) (WT Con: n = 48 dendrites from 5 mice; APP/PS1 Con: n = 64 dendrites from 5 mice; APP/PS1 KYL: n = 59 dendrites from 5 mice; ***P < 0.001; one-way ANOVA followed by post hoc Tukey's test). (*J*) Input–output curves showing the FV amplitude vs. stimulus amplitude (*P < 0.05, two-way repeated measure ANOVA). (*K*) Input–output curves showing the fEPSP slopes vs. stimulus amplitude (**P < 0.01, two-way repeated measure ANOVA). (*L* and *M*) Measurement of hippocampal LTP in 12-mo-old APP/PS1 mice after KYL treatment. (*L*) Points represent averaged fEPSP slopes normalized to baseline. Trace recordings 5 min before (1) and 50 min after (2) LTP induction (arrow) are shown. (*M*) Quantification of mean fEPSP slopes in the last 10 min of recording after the induction of LTP (WT Con: n = 24 slices from 9 mice, APP/PS1 Con: n = 16 slices from 7 mice, APP/PS1 KYL: n = 16 slices from 8 mice; *P < 0.05; one-way ANOVA followed by post hoc Tukey's test). Data are mean ± SEM.

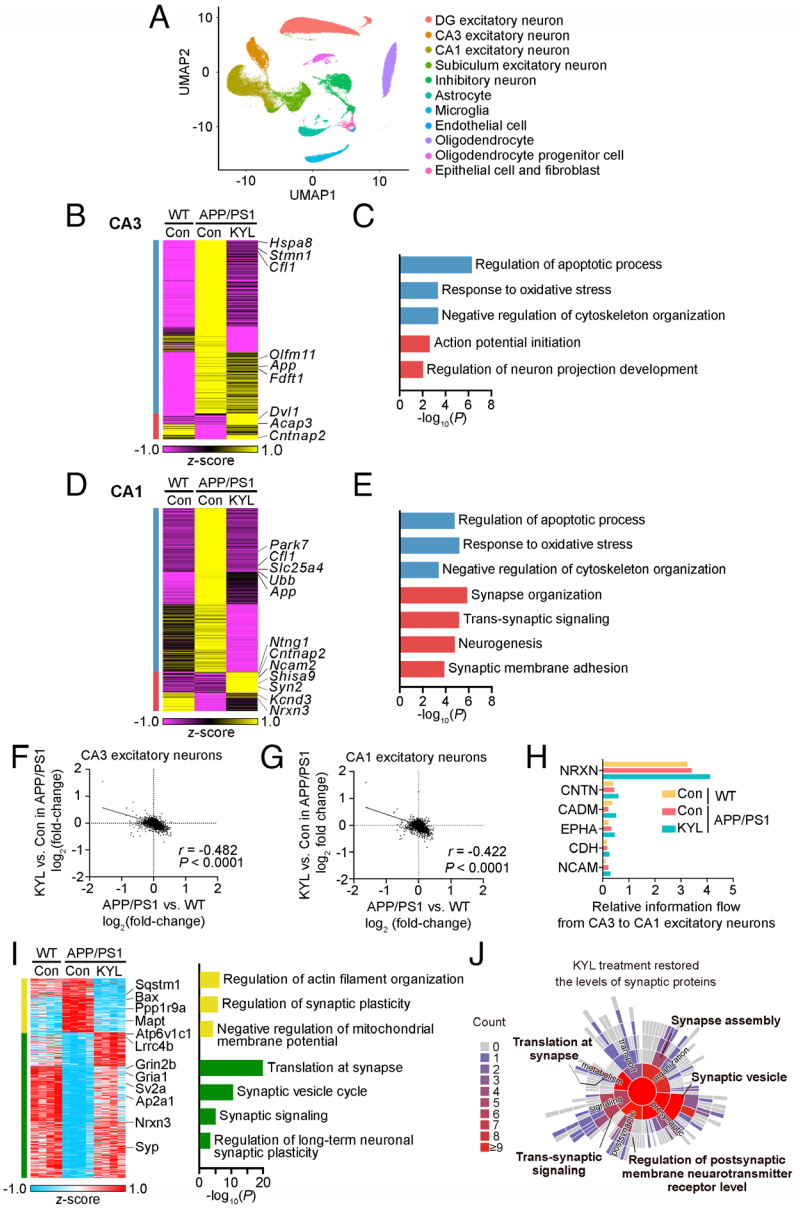

Fig. 4. Blockade of EphA4 signaling strengthens synaptic connectivity between CA3 and CA1 excitatory neurons in APP/PS1 mice. (*A*) Unbiased identification of cell types in the mouse hippocampus. Uniform manifold approximation and projection (UMAP) plot showing 11 cell types identified in a total of 91,845 nuclei from all samples. (*B*) Heatmap showing the DEGs that exhibited modulation in KYL-treated APP/PS1 mice in CA3 excitatory neurons (APP/PS1 KYL vs. APP/PS1 Con and APP/PS1 Con vs. wild-type [WT] Con mice). (*C*) Bar chart showing results of GO analysis of the blue and red clusters of the heatmap in (*B*). (*D*) Heatmap showing the DEGs that exhibited modulation in KYL-treated APP/PS1 mice in CA1 excitatory neurons (APP/PS1 KYL vs. APP/PS1 Con mice and APP/PS1 Con vs. WT Con mice). (*E*) Bar chart showing the results of GO analysis of the red cluster of heatmap in (*D*). (*F*) Negative correlation of changes in the CA3 excitatory neuron transcriptome profile of APP/PS1 KYL vs. APP/PS1 Con mice and APP/PS1 Con vs. WT Con mice ($r = -0.482$, $P < 0.0001$). (*G*) Negative correlation of changes in the CA1 excitatory neuron transcriptome profile of APP/PS1 KYL vs. APP/PS1 Con mice and APP/PS1 Con vs. WT Con mice ($r = -0.422$, $P < 0.0001$). (*H*) Bar chart showing the communication strengths of the top pathways between CA3 and CA1 excitatory neurons identified by CellChat. (*I*) Heatmap showing the clustered differentially expressed proteins (DEPs) in the hippocampal synaptosome in APP/PS1 KYL vs. APP/PS1 Con mice. *Right*: Bar chart showing the results of GO analysis of the DEPs in yellow and green clusters in the heatmap on the *Left*, respectively. (*J*) Sunburst plot from SynGO showing the restored synaptic proteins in APP/PS1 mice after KYL treatment [green cluster in (*I*)]; proteins are classified according to their biological functional identities.

returned to the levels observed in the WT control mice (Fig. 4 *B*–*E*). Thus, these findings suggest that KYL treatment increases neuronal survival in APP/PS1 mice.

Meanwhile, the CA3 neurons of KYL-treated APP/PS1 mice exhibited upregulation of a gene cluster associated with "action potential initiation" and "neuron projection development" (red cluster in Fig. 4 *B* and *C*). In contrast, a gene cluster related to "synapse organization" and "synaptic signaling" was up-regulated in the CA1 neurons in these mice (red cluster in Fig. 4 *D* and *E*). Overall analysis of the transcriptomic changes in both neuronal populations showed that the changes in APP/PS1 mice following KYL treatment were inversely related to those in the APP/PS1 control mice vs. the WT control mice (Fig. 4 *F* and *G*). This suggests that KYL treatment in APP/PS1 mice restores the gene expression patterns in both CA3 and CA1 neurons to levels comparable to those in the WT mice. Together, these findings suggest that EphA4 inhibition in APP/PS1 mice reverses the molecular alterations associated with synapse organization and functions in presynaptic CA3 and postsynaptic CA1 excitatory neurons, restoring them to levels observed in the WT mice and thereby potentially enhancing synaptic communication in the SC–CA1 pathway in AD.

Concordantly, analysis of receptor–ligand interactions between CA3 and CA1 excitatory neurons using CellChat (45) identified key pathways related to synaptic cell adhesion signalings, such as heterophilic neurexin–neuroligin (NRXN) and homophilic signaling contactin (CNTN), which are crucial facilitators of the recovery of functional synapses (Fig. 4*H*). In particular, the communication strengths of these pathways were elevated in APP/PS1 mice after KYL treatment.

To better understand the structural and functional changes of synapses in the hippocampus in APP/PS1 mice following KYL treatment, we conducted proteomic analysis of the hippocampal synaptosomes from the WT control, APP/PS1 control, and KYL-treated APP/PS1 mice. The differentially expressed proteins in APP/PS1 mice upon KYL treatment included 122 down-regulated and 328 up-regulated proteins (yellow and green clusters, respectively, in Fig. 4*I* and Dataset S3). In KYL-treated APP/PS1 mice, GO analysis revealed that inhibition of EphA4 signaling regulates both pre- and postsynaptic components (Fig. 4*I*). Furthermore, Synaptic Gene Ontologies (SynGO) analysis showed that synaptic proteins related to translation at synapses, synaptic vesicle endocytosis, and postsynaptic specialization assembly were up-regulated

in KYL-treated APP/PS1 mice (green cluster in Fig. 4 *I* and *J*). Thus, these findings show that inhibition of EphA4 signaling restores the levels of proteins associated with synaptic functions and structures.

EphA4 Inhibition Decreases Astrocyte Reactivity in Alzheimer's Disease Transgenic Mouse Models. Given the critical role of astrocytic EphA4 in mediating the hippocampal excitatory synapse loss in AD (Fig. 2 and *SI Appendix*, Fig. S5), we examined how EphA4 blockade modulates the molecular phenotypes of astrocytes by transcriptomic analysis in our snRNA-seq dataset. Compared to the APP/PS1 control mice, KYL treatment in APP/PS1 mice led to decreased expression of astrocytic genes associated with mitochondrial organization and functions, including oxidative phosphorylation and ATP synthesis (blue cluster in Fig. 5 *A* and *B*). This suggests that EphA4 inhibition alters the metabolic state of astrocytes in AD; such a change is strongly correlated with astrocytic hyperreactivity and subsequent neuronal damage (46–48).

Astrocytes are heterogeneous and dynamically alter their phenotypes and functions in response to the microenvironment, especially in disease contexts (49, 50). To examine how EphA4 inhibition regulates the molecular phenotype of astrocytes, we conducted unbiased cluster analysis of the transcriptomic profiles of hippocampal astrocytes from WT control, APP/PS1 control, and KYL-treated APP/PS1 mice at the single-nucleus level. Accordingly, we identified 3 distinct astrocyte subpopulations—designated Astro1, Astro2, and Astro3—each characterized by specific marker genes (Fig. 5 *C* and *D* and Dataset S4). Astro1 resembled a previously reported homeostatic astrocyte subpopulation (49) marked by the calcium channel protein *Trpm3* and the leucine zipper protein *Luzp2*. The Astro2 subcluster was characterized by markers such as the glycoprotein thrombospondin *Thbs4*, the netrin receptor *Dcc*, the microsomal enzyme *Hsd11b1*, the Eph family member *Ephb1*, and the protein neddylation regulator *Dcun1d4*, suggesting a role in dynamic polarity and protein metabolism. Last, the Astro3 subcluster exhibited enriched expression of the cytoskeleton glycoprotein regulator *Myoc*, the transcription factor *Id3*, and the intermediate filaments *Gfap* and *Vim* (Dataset S4), indicating reactive astrocytes associated with AD pathology (49, 51, 52). Notably, the Astro3 subpopulation exhibited higher expression of the *Epha4* transcript and genes associated with synapse elimination and phagocytosis (Fig. 5 *E* and *F*) (50, 53–57). Moreover, Astro3 was enriched in genes that are markers

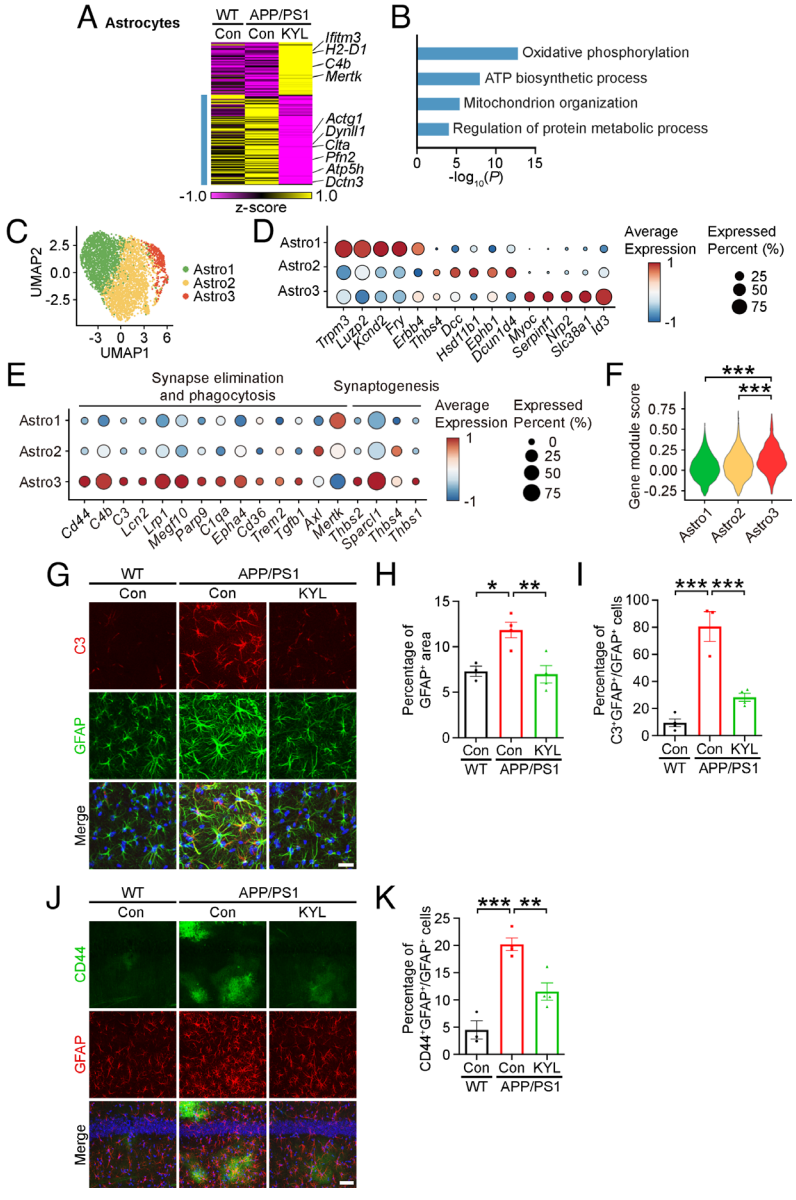

Fig. 5. Astrocyte reactivity decreases upon KYL treatment. (*A*) Heatmap showing the DEGs that exhibited modulation in KYL-treated APP/PS1 mice in astrocytes (APP/PS1 KYL vs. APP/PS1 Con and APP/PS1 Con vs. WT Con mice). (*B*) Bar chart showing the GO analysis results of the blue cluster in (*A*). (*C*) UMAP plot showing 3 astrocyte subtypes from unbiased clustering of all astrocytes from the WT Con, APP/PS1 Con, and APP/PS1 KYL groups. (*D*) Dot plot showing the top unique markers of the three clusters ranked by *P*-value. (*E*) Dot plot showing the expression of candidate genes related to synapse elimination, phagocytosis, and synaptogenesis in astrocyte subclusters. (*F*) Violin plot showing the module scores of the 3 astrocyte subtypes expressing genes in (*E*) (Wilcoxon test). (*G–I*) Immunohistochemical analysis of C3 and GFAP in the hippocampal CA1 region of 12-mo-old APP/PS1 mice after KYL treatment. (*G*) Representative images of reactive astrocytes costained with C3 (red) and GFAP (green) in the hippocampal CA1 region. (Scale bar: 25 μm.) (*H*) Quantitative analysis of the percentage of the $GFAP^+$ area in the hippocampal CA1 region. (*I*) Quantitative analysis of the percentage of $C3^+GFAP^+$ astrocytes among total $GFAP^+$ astrocytes in the hippocampal CA1 region (n = 4, 3–4, and 4 mice for WT Con, APP/PS1 Con, and APP/PS1 KYL, respectively; $^{**}P < 0.01$ and $^{***}P < 0.001$; one-way ANOVA followed by post hoc Tukey's test). (*J* and *K*) Immunohistochemical analysis of CD44 in the hippocampal CA1 region of 12-mo-old APP/PS1 mice after KYL treatment. (*J*) Representative images of astrocytes costained with CD44 (green) and GFAP (red) in the hippocampal CA1 region. (Scale bar: 50 μm.) (*K*) Quantification of the percentage of $CD44^+GFAP^+$ astrocytes among total $GFAP^+$ astrocytes in the hippocampal CA1 region (n = 3, 4, and 4 mice for WT Con, APP/PS1 Con, and APP/PS1 KYL, respectively; $^{***}P < 0.001$ and $^{**}P < 0.01$; one-way ANOVA followed by post hoc Tukey's test). Data are mean ± SEM.

of reactive astrocytes (e.g., *Cd44*, *C4b*, *C3*, and *Lcn2*) (49–51, 58–60), suggesting a role of astrocytic EphA4 in the upregulation of astrocyte reactivity.

Of note, C3, a principal component of the complement pathway, is a direct downstream effector of C1q, whose activation triggers astrocytes to be in a reactive state (58). CD44, a cell surface glycoprotein present in reactive astrocytes (50, 61), also acts as a receptor for C1q (62). Importantly, C3 mediates synapse engulfment by glial cells (24, 26, 63, 64). Accordingly, blockade of EphA4 signaling reduced the GFAP$^+$ area and ameliorated the elevated GFAP immunoreactivity in the hippocampus in APP/PS1 mice, as indicated by thinner main processes and reduced proximal processes (Fig. 5 *G* and *H*), suggesting decreased astrocyte reactivity. Moreover, KYL treatment led to a lower percentage of C3$^+$ astrocytes and CD44$^+$ astrocytes in APP/PS1 mice (Fig. 5 *G*–*K*). Together, these results indicate that EphA4 inhibition reduces astrocyte reactivity and the downstream effectors of C1q in the hippocampal CA1 region in AD, suggesting a role of EphA4 in the regulation of C1q-mediated effects on synapses.

EphA4 Inhibition Decreases Excitatory Synapse Engulfment by Astrocytes in Alzheimer's Disease. The elimination of excitatory synapses by astrocytes in AD is dependent on C1q (24). C1q is pivotal for target recognition and initiates the classical complement pathway to induce astrocytic elimination of synapse (22, 24, 58, 65). Therefore, we examined the effect of KYL treatment on the C1q tagging of synapses. C1q level in the hippocampus and colocalization of C1q and PSD-95 were significantly greater in the APP/PS1 control mice than the WT control mice (Fig. 6 *A*–*C*). However, following KYL treatment in APP/PS1 mice, both the level of C1q and its colocalization with PSD-95 decreased significantly (Fig. 6 *A*–*C*), suggesting decreased tagging of PSD-95 by C1q.

Such a decrease in C1q tagging on excitatory synapses in CA1 neurons in KYL-treated APP/PS1 mice suggests decreased synapse engulfment activity by astrocytes. Therefore, we examined the presence of the synaptic component, PSD-95, within astrocytes in the hippocampal CA1 region. Compared to the WT control mice, reactive astrocytes in the APP/PS1 mice exhibited increased cytosolic volume and thickening of main processes together with more internalized PSD-95 puncta (Fig. 6 *D* and *E*). Meanwhile, KYL treatment in APP/PS1 mice led to reductions in both the cytosolic volume of astrocytes and the number of internalized PSD-95 puncta, suggesting diminished hyperreactivity and synapse engulfment by astrocytes (Fig. 6 *D*–*F*). Thus, these results collectively suggest a critical role of EphA4 signaling in the removal of excitatory synapses by astrocytes in the hippocampal CA1 region.

Astrocytic EphA4 Is Important for Astrocyte Activation and Excitatory Synapse Engulfment in Alzheimer's Disease. Next, we investigated whether astrocytic EphA4 specifically influences astrocyte reactivity and synapse engulfment in the hippocampus in APP/PS1 mice. EphA4 knockout in astrocytes in APP/PS1 mice led to decreased astrocyte reactivity, as indicated by a smaller proportion of C3$^+$ astrocytes (Fig. 7 *A* and *B*) and fewer C1q-colocalized PSD-95 puncta (Fig. 7 *C* and *D*); this suggests a diminished signal for synapse engulfment by astrocytes. In contrast, EphA4 knockout in the hippocampal CA1 neurons of APP/PS1 mice did not alter astrocyte reactivity (Fig. 7 *A* and *B*) or the percentage of C1q-colocalized PSD-95 puncta (Fig. 7 *C* and *D*). This suggests that neuronal EphA4 does not contribute to astrocyte reactivity or complement-dependent synapse engulfment in AD. Moreover, specific knockout of EphA4 in astrocytes and not neurons resulted in significant decreases in both the cytoplasmic

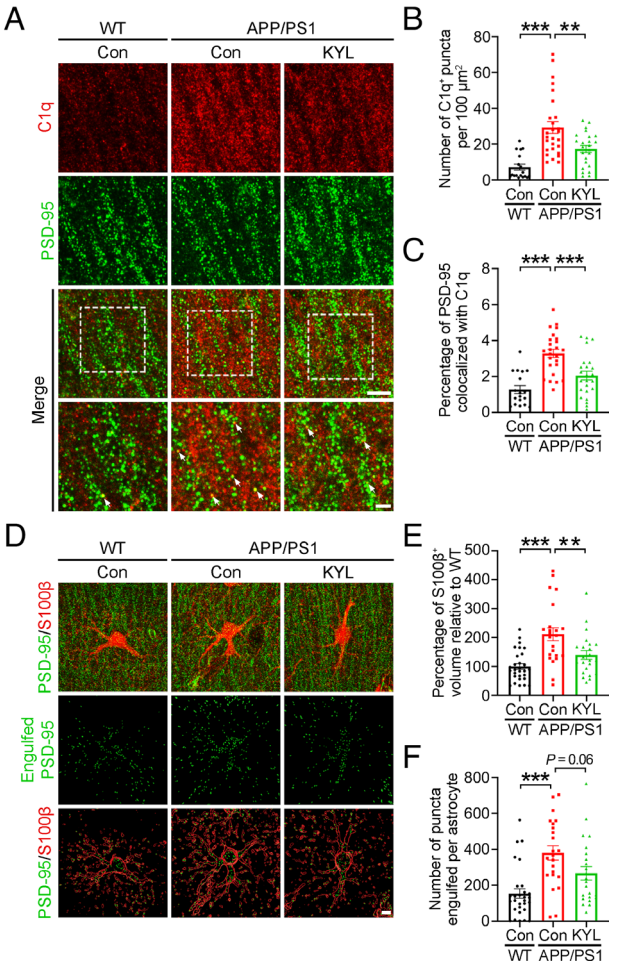

Fig. 6. Blockade of EphA4 signaling decreases C1q tagging on synapses and astrocytic engulfment of synaptic proteins in APP/PS1 mice. (*A*–*C*) Immunohistochemical analysis of C1q protein expression and tagging on PSD-95 in the hippocampal CA1 region of 12-mo-old APP/PS1 mice after KYL treatment. (*A*) Representative images showing C1q and PSD-95 (*Top* and *Bottom* scale bars: 5 and 2 μm, respectively). (*B*) Quantitative analysis of C1q$^+$ puncta density and (*C*) percentage of PSD-95 colocalized with C1q in the hippocampal CA1 region (WT Con: n = 18 astrocytes from 5 mice, APP/PS1 Con: n = 27 astrocytes from 6 mice, APP/PS1 KYL: n = 24 astrocytes from 5 mice; ***P < 0.001 and **P < 0.01; one-way ANOVA followed by post hoc Tukey's test). (*D*–*F*) Immunohistochemical analysis of the level of PSD-95 engulfed by astrocytes in the hippocampal CA1 region of 12-mo-old APP/PS1 mice after KYL treatment. (*D*) Representative images and 3D reconstruction including overlay of S100β and PSD-95 staining in the hippocampal CA1 region. (Scale bar: 5 μm.) (*E*) Quantification of S100β$^+$ volume relative to the WT Con group. (*F*) Quantification of PSD-95 puncta inside astrocytes in the hippocampal CA1 region (WT Con: n = 29 astrocytes from 6 mice, APP/PS1 Con: n = 23 astrocytes from 5 mice, APP/PS1 KYL: n = 24 astrocytes from 5 mice; ***P < 0.001 and **P < 0.01; one-way ANOVA followed by post hoc Tukey's test). Data are mean ± SEM.

volume of astrocytes and PSD-95 content within astrocytes (Fig. 7 *E*–*G*). Together, these findings indicate that astrocytic EphA4 signaling plays a crucial role in mediating astrocyte reactivity and excitatory synapse engulfment by astrocytes, suggesting that EphA4 signaling contributes to excitatory synapse loss in the hippocampal CA1 region in APP/PS1 mice.

Discussion

Hippocampal synapse loss and synaptic dysfunction due to neuronal damage and glial cell malfunction are key contributors to cognitive impairment in patients with AD. While certain cell surface receptors regulate synaptic dysfunctions in AD, their roles in specific cell types are largely unclear. In this study, we revealed

the crucial roles of astrocytic EphA4 in hippocampal synaptic dysfunction in AD. Of note, we showed that astrocytic EphA4 plays a vital role in mediating hippocampal synapse loss in AD. Our findings indicate that astrocytic EphA4 is important for the astrocyte reactivity and complement signaling activation in AD. Moreover, we showed that EphA4 is important for the engulfment of complement-associated excitatory synapses by astrocytes in AD. This study demonstrates the role of astrocytic EphA4 in synaptic dysregulation in the hippocampus under AD conditions. Indeed, dysregulation of EphA4 expression is observed in postmortem patient brain (66), and this supports our findings in the role of EphA4 in synaptic dysfunction in AD.

Astrocyte-mediated synapse elimination is a crucial mechanism for sculpting neural circuits, particularly during postnatal development and continuing in an activity-dependent manner in adulthood in rodents (29). However, our understanding of the molecular mechanisms that regulate the expression of phagocytic signaling in astrocytes remains limited. In the current study, we highlight the role of astrocytic EphA4 in complement-mediated synapse elimination within the context of AD. Our previous studies also demonstrate that EphA4 signaling is involved in the loss of excitatory synapses induced by soluble Aβ in hippocampal neurons (35). Furthermore, neuronal EphA4, which can be activated by a chronic increase in neuronal activity, plays an important role in the retraction of dendritic spines and downregulation of AMPA receptors during homeostatic plasticity (36, 38). Given that EphA4 is present in CA1 astrocytes at low levels under physiological conditions, astrocytic EphA4 may be activated and influence synapse elimination in response to changes in neuronal activity. Our snRNA-seq results reveal the heterogeneity of astrocytes under AD conditions. Specifically, the Astro3 astrocyte subpopulation, which highly expresses *Epha4*, resembles and shares several markers with the disease-associated or hyperreactive astrocytes identified in AD transgenic mouse models (49, 51, 52). Such disease-associated astrocytes emerge from homeostatic astrocytes and are associated with amyloid plaques (49, 50). Consistent with previous studies showing that EphA4 signaling is activated in response to Aβ in AD (35) and that *Epha4*$^{+}$ astrocytes may have neurotoxic properties and decrease neuronal survival (58), it is of interest to investigate whether *Epha4* is a marker of disease-associated astrocytes

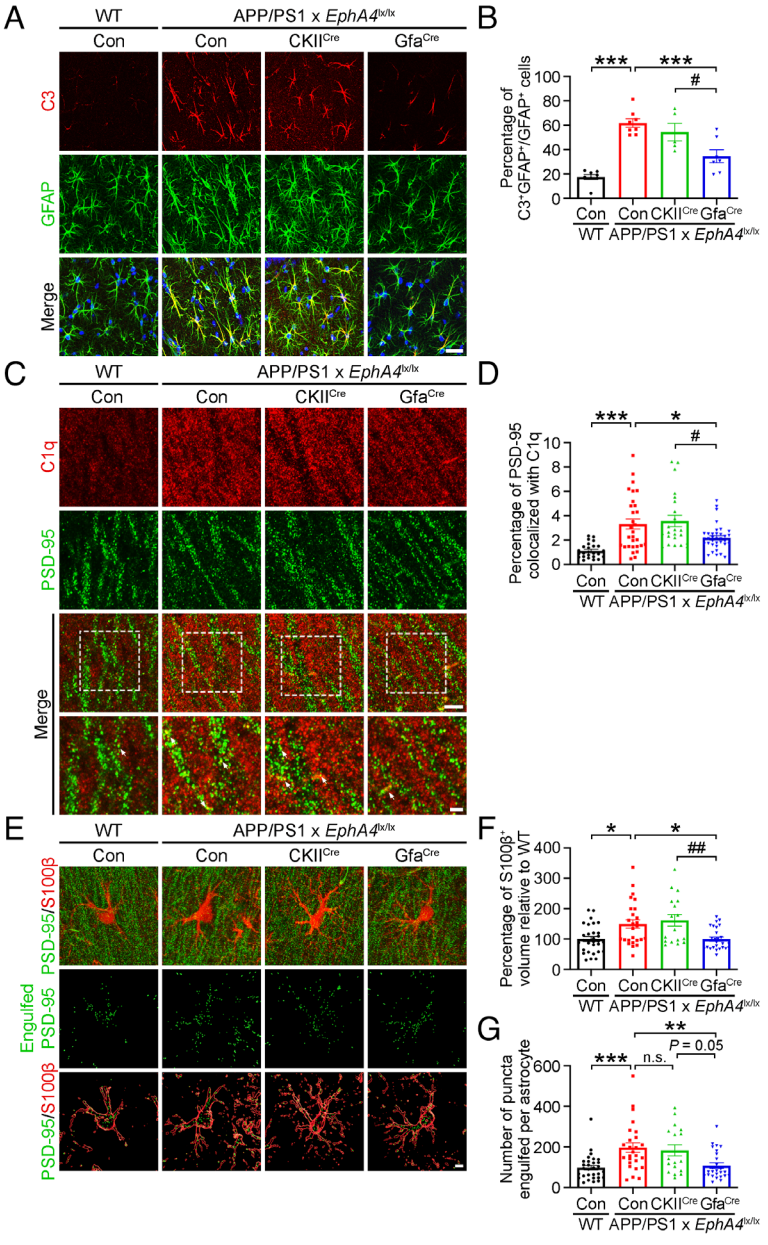

Fig. 7. Deletion of astrocytic EphA4 decreases C1q tagging on PSD-95 and astrocytic engulfment of synaptic proteins. (*A* and *B*) Immunohistochemical analysis of C3 in the hippocampal CA1 region of 12-mo-old APP/PS1 × EphA4$^{lx/lx}$ mice after conditional knockout of neuronal or astrocytic EphA4 in the hippocampal CA1 region. (*A*) Representative images of reactive astrocytes labeled by costaining with C3 (red) and GFAP (green) in the hippocampal CA1 region of APP/PS1 × EphA4$^{lx/lx}$ mice. (Scale bar: 25 μm.) (*B*) Quantification of C3^{+}GFAP^{+} astrocytes among total GFAP^{+} astrocytes in the hippocampal CA1 region (WT × EphA4$^{lx/lx}$ AAV9-CaMKIIa [Con]: n = 8 mice, APP/PS1 × EphA4$^{lx/lx}$ Con: n = 8 mice, APP/PS1 × EphA4$^{lx/lx}$ AAV9-CaMKIIa-Cre [CKII^{Cre}]: n = 5 mice, APP/PS1 × EphA4$^{lx/lx}$ AAV9-GfaABC1D-Cre [Gfa^{Cre}]: n = 7 mice; one-way ANOVA followed by post hoc Tukey's test). (*C* and *D*) Immunohistochemical analysis of C1q protein expression and tagging on PSD-95 in the hippocampal CA1 region. (*C*) Representative images, including overlay images showing C1q and PSD-95 (*Top* and *Bottom* scale bars: 5 and 2 μm, respectively). (*D*) Quantitative analysis of the percentage of PSD-95 colocalized with C1q in the hippocampal CA1 region (WT × EphA4$^{lx/lx}$ Con: n = 4 mice, APP/PS1 × EphA4$^{lx/lx}$ Con: n = 5 mice, APP/PS1 × EphA4$^{lx/lx}$ CKII^{Cre}: n = 4 mice, APP/PS1 × EphA4$^{lx/lx}$ Gfa^{Cre}: n = 6 mice; $^{*}P < 0.05$, $^{***}P < 0.001$, and $^{\#}P < 0.05$; one-way ANOVA followed by post hoc Tukey's test). (*E*–*G*) Immunohistochemical analysis of the level of PSD-95 engulfed by astrocytes in the hippocampal CA1 region of APP/PS1 × EphA4$^{lx/lx}$ mice. (*E*) Representative images and 3D reconstruction including overlay of S100β and PSD-95 in the hippocampal CA1 region. (Scale bar: 5 μm.) (*F*) Quantification of S100β^{+} volume relative to that of WT mice. (*G*) Quantification of PSD-95 puncta inside astrocytes (WT × EphA4$^{lx/lx}$ Con: n = 30 astrocytes from 6 mice, APP/PS1 × EphA4$^{lx/lx}$ Con: n = 26 astrocytes from 5 mice, APP/PS1 × EphA4$^{lx/lx}$ CKII^{Cre}: n = 17 astrocytes from 4 mice, APP/PS1 × EphA4$^{lx/lx}$ Gfa^{Cre}: n = 26 astrocytes from 6 mice; $^{*}P < 0.05$, $^{**}P < 0.01$, $^{\#}P < 0.05$, and $^{\#\#}P < 0.01$; one-way ANOVA followed by post hoc Tukey's test). Data are mean ± SEM.

that surround with Aβ in the hippocampus in AD transgenic mouse models.

Although astrocytes are the predominant cell type involved in the elimination of excitatory synapses in the hippocampus in AD (24), the cellular receptor signaling that governs this process was unknown. Consistent with a report showing that synapse engulfment by astrocytes is associated with astrocyte reactivity (27), the present study shows that astrocytic EphA4 signaling is important for astrocyte reactivity and synapse elimination in AD. Astrocytic EphA4 is also activated and regulates astrocyte reactivity in other pathological contexts (40, 41). Therefore, EphA4 may be a key signaling activator that triggers astrogliosis, which leads to increased synapse engulfment by astrocytes (28, 67).

To become activated, Eph receptors must interact with their ligands, Ephrins (68). However, it is unknown which Ephrins interact with astrocytic EphA4 to stimulate astrocyte reactivity and excitatory synapse elimination. EphA4 can potentially interact with all Ephrins, including 6 Ephrin-As and 3 Ephrin-Bs (69). To date, only Ephrin-A5 has been identified as a ligand for astrocytic EphA4, which induces astrogliosis after brain injury in marmosets (41), making it a potential candidate activator of astrocytic EphA4 in the mouse hippocampus. As Eph–Ephrin interactions trigger bidirectional signaling, astrocytic EphA4 likely activates reverse Ephrin signaling in neighboring Ephrin-expressing cells. Our findings show that astrocytic EphA4 regulates the hippocampal level of C1q, which is mainly released by microglia and affects synapse elimination by astrocytes (24, 70). Therefore, astrocytic EphA4 may interact with Ephrins residing on microglia in AD.

There are some potential mechanisms by which astrocytic EphA4 regulates astrocyte reactivity. Given that EphA4 activates STAT3 (71), a transcription factor necessary for astrogliosis induced by Aβ oligomers and proinflammatory cytokines (72), astrocytic EphA4 potentially regulates astrocyte reactivity via STAT3 signaling. Accordingly, STAT3 activation is crucial for the expression of reactive astrocyte markers (e.g., C3, GFAP, and vimentin) (73–75). In the current study, we also observed that inhibition of EphA4 signaling reduced the oxidative process and metabolic stress in astrocytes, which may be due to decreased STAT3 activation (76, 77). Coincidentally, our results show significant enrichment of *Stat3* exclusively in the Astro3 subpopulation (Dataset S4), which exhibited relatively high expression of *Epha4*. In addition, EphA4 activation may trigger the downstream effectors, MAPK and Rho, to modulate cytoskeleton reorganization in astrocytes (41, 78), resulting in astrocyte hypertrophy and increased synapse engulfment. This is concordant with our observation that the inhibition of astrocytic EphA4 signaling reduced the cytoplasmic volume of $S100\beta^+$ astrocytes and area of $GFAP^+$ intermediate filaments. However, further investigation is required to determine whether the activation of astrocytic EphA4 induces these intracellular signaling pathways and whether astrocytic EphA4 affects the phagocytosis and degradation of engulfed proteins.

Activated microglia are thought to initiate the immune response by releasing proinflammatory signals to induce astrocyte activation and trigger their excessive elimination of synapses in AD (24, 58, 79). However, in the present study, we showed that deletion of astrocytic EphA4 resulted in a significant reduction of astrocytic synapse elimination. Nonetheless, it is interesting to examine whether astrocytes will coordinate with microglia to eliminate synapses, which is concordant with the reported astrocyte–microglia communication under AD conditions (80).

In summary, we demonstrated that astrocytic EphA4 specifically regulates astrocyte reactivity, complement signaling activation, and the elimination of excitatory synapses in AD. Given that astrocytic EphA4 is an important regulator of the hippocampal synapse loss in AD, deletion of astrocytic EphA4 may limit the elimination of excitatory synapses from the brain. Therefore, limiting neurotoxic processes, such as synaptic pruning, by attenuating astrocytic EphA4 may be a promising strategy for AD therapeutic development.

Methods and Materials

For details about the methods and materials, please see *SI Appendix, SI Materials, and Methods*.

Animals. All transgenic mice were housed in the Laboratory Animal Facility of the Hong Kong University of Science and Technology (HKUST), and all experiments were conducted in accordance with guidelines and regulations approved by the Animal Ethics Committee of HKUST.

In Situ Hybridization by RNAscope and Image Analysis. We performed in situ hybridization RNAscope on APP/PS1 and 5XFAD mice.

Immunohistochemical and Imaging Analysis. We used antibodies for Cre, GFAP, PSD-95, VGluT1, C3, C1q, CD44, and S100β for immunostaining.

Peptide Infusion and Stereotactic Virus Injection. We implanted the mice with mini-osmotic pumps to block EphA4 signaling with KYL peptide. We injected Cre viruses into the hippocampal CA1 region of AD transgenic mouse models to examine the cellular role of EphA4.

Electrophysiology. We performed input–output curve and LTP recordings as previously described (35).

Nucleus Isolation and Single-Nucleus RNA-seq Library Preparation. We isolated nuclei from frozen hippocampal samples of APP/PS1 mice and prepared the snRNA-seq libraries as previously described (81).

Single-Nucleus RNA-seq Analysis. We performed transcriptome analysis on hippocampal samples of mice treated with KYL for 3 to 4 wk.

Synaptosome Preparation. We prepared synaptosomes from the hippocampal samples of mice treated with KYL for 3 to 4 wk.

Liquid Chromatography–Mass Spectrometry and Analysis of the Synaptosome. We injected the samples into a nanoElute LC system (Bruker) and analyzed the eluted peptides using a TimsTOF Pro (Bruker) in DDA mode.

Mass Spectrometry and Analysis of the Synaptosome. Mass spectral data were assigned to peptides using UniProtKB/UniProt (82) in FragPipe (version V20.0) (83–85). We performed synaptosomal biological functional classification using SynGO (86).

Statistical Analysis. All data are expressed as mean ± SEM. We assessed the significance of differences by unpaired two-tailed Student's *t* test or one-way ANOVA followed by a post hoc Tukey test as indicated. The level of significance was as follows: $^*P < 0.05$, $^{**}P < 0.01$, and $^{***}P < 0.001$. We used linear regression in the correlation analysis. We performed all statistical analysis using GraphPad Prism (version 8.4.0). Data showed no significant differences between sexes.

Data, Materials, and Software Availability. The snRNA-seq dataset is deposited on Gene Expression Omnibus (GEO) with accession number GSE284797, and the mass spectrometry dataset is deposited to the ProteomeXchange Consortium via the PRIDE (87) partner repository with the dataset identifier PXD056771. The marker genes of clusters in snRNA-seq datasets are provided in Dataset S1. The DEGs in CA3 and CA1 excitatory neurons are provided in Dataset S2. The differentially expressed proteins in the synaptosome (APP/PS1 KYL vs. APP/PS1 con) are provided in Dataset S3. The marker genes of astrocyte subclusters are provided in Dataset S4.

ACKNOWLEDGMENTS. We thank E. Tam, C. Kwong, K.C. Lok, P.O. Chiu, S.F. Lau, C.C. Yip, R. Delos Reyes, and S. To for their technical assistance and other members of the Ip laboratory for their helpful discussions. We thank the Biosciences Central Research Facility, HKUST for the use of mass spectrometry instruments and services. We thank the Laboratory Animal Facility, HKUST for housing and caring for the mice used in this study. This study was supported in part by the National Key Research and Development Program of China grant (2021YFE0203000); the Research Grants Council of Hong Kong (the Collaborative Research Fund [C6027-19GF] and the Theme-Based Research Scheme [T13-605/18W]) and the General Research Fund [HKUST16102019]); the Areas of Excellence Scheme of the University Grants Committee (AoE/M-604/16); the Innovation and Technology Commission (InnoHK [INNOHK18SC01] and Grant [ITCPD/17-9]); and the Fundamental Research Program of Shenzhen Virtual University Park (2021Szvup137). The funders had no role in study design, data collection or analysis, decision to publish, or preparation of the manuscript.

Author affiliations: [a]Division of Life Science, State Key Laboratory of Molecular Neuroscience, Daniel and Mayce Yu Molecular Neuroscience Center, The Hong Kong University of Science and Technology, Hong Kong Special Administrative Region, China; [b]Hong Kong Center for Neurodegenerative Diseases, Hong Kong Science Park, Hong Kong Special Administrative Region, China; and [c]Guangdong Provincial Key Laboratory of Brain Science, Disease and Drug Development, Hong Kong University of Science and Technology Shenzhen Research Institute, Shenzhen-Hong Kong Institute of Brain Science, Shenzhen, Guangdong 518057, China

Author contributions: X.Y., Y.W., Y.Q., J.L., W.-Y.F., A.K.Y.F., and N.Y.I. designed research; X.Y., Y.W., Y.Q., and J.L. performed research; N.Y.I. contributed new reagents/analytic tools; X.Y., Y.W., Y.Q., W.-Y.F., A.K.Y.F., and N.Y.I. analyzed data; and X.Y., Y.Q., J.K.Y.L., W.-Y.F., A.K.Y.F., and N.Y.I. wrote the paper.

1. P. Penzes, M. E. Cahill, K. A. Jones, J.-E. VanLeeuwen, K. M. Woolfrey, Dendritic spine pathology in neuropsychiatric disorders. *Nat. Neurosci.* **14**, 285–293 (2011).
2. S. E. Kwon, E. R. Chapman, Synaptophysin regulates the kinetics of synaptic vesicle endocytosis in central neurons. *Neuron* **70**, 847–854 (2011).
3. H. W. Querfurth, F. M. LaFerla, Alzheimer's disease. *N. Engl. J. Med.* **362**, 329–344 (2010).
4. A. Kobro-Flatmoen *et al.*, Re-emphasizing early Alzheimer's disease pathology starting in select entorhinal neurons, with a special focus on mitophagy. *Ageing Res. Rev.* **67**, 101307 (2021).
5. M. Hernández-Frausto, C. Vivar, Entorhinal cortex–hippocampal circuit connectivity in health and disease. *Front. Hum. Neurosci.* **18**, 1448791 (2024).
6. G. Neves, S. F. Cooke, T. V. P. Bliss, Synaptic plasticity, memory and the hippocampus: A neural network approach to causality. *Nat. Rev. Neurosci.* **9**, 65–75 (2008).
7. C. Dong, A. D. Madar, M. E. J. Sheffield, Distinct place cell dynamics in CA1 and CA3 encode experience in new environments. *Nat. Commun.* **12**, 2977 (2021).
8. D. M. Smith, D. A. Bulkin, The form and function of hippocampal context representations. *Neurosci. Biobehav. Rev.* **40**, 52–61 (2014).
9. S. G. Jeon, Y. J. Kim, K. A. Kim, I. Mook-Jung, M. Moon, Visualization of altered hippocampal connectivity in an animal model of Alzheimer's disease. *Mol. Neurobiol.* **55**, 7886–7899 (2018).
10. Q. Ye *et al.*, Hippocampal neural circuit connectivity alterations in an Alzheimer's disease mouse model revealed by monosynaptic rabies virus tracing. *Neurobiol. Dis.* **172**, 105820 (2022).
11. Y. Yang *et al.*, Amyloid-β oligomers may impair SNARE-mediated exocytosis by direct binding to syntaxin 1a. *Cell Rep.* **12**, 1244–1251 (2015).
12. J. Marsh, P. Alifragis, Synaptic dysfunction in Alzheimer's disease: The effects of amyloid beta on synaptic vesicle dynamics as a novel target for therapeutic intervention. *Neural Regen. Res.* **13**, 616 (2018).
13. E. H. Chang *et al.*, AMPA receptor downscaling at the onset of Alzheimer's disease pathology in double knockin mice. *Proc. Natl. Acad. Sci. U.S.A.* **103**, 3410–3415 (2006).
14. S. Guntupalli, J. Widagdo, V. Anggono, Amyloid- β-induced dysregulation of AMPA receptor trafficking. *Neural Plast.* **2016**, 1–12 (2016).
15. H. Hsieh *et al.*, AMPAR removal underlies Aβ-induced synaptic depression and dendritic spine loss. *Neuron* **52**, 831–843 (2006).
16. A. J. Miñano-Molina *et al.*, Soluble oligomers of amyloid-β peptide disrupt membrane trafficking of α-amino-3-hydroxy-5-methylisoxazole-4-propionic acid receptor contributing to early synapse dysfunction. *J. Biol. Chem.* **286**, 27311–27321 (2011).
17. Y. Chen, A. K. Y. Fu, N. Y. Ip, Synaptic dysfunction in Alzheimer's disease: Mechanisms and therapeutic strategies. *Pharmacol. Ther.* **195**, 186–198 (2019).
18. P. Kurup *et al.*, Aβ-mediated NMDA receptor endocytosis in Alzheimer's disease involves ubiquitination of the tyrosine phosphatase STEP 61. *J. Neurosci.* **30**, 5948–5957 (2010).
19. J. Griffiths, S. G. N. Grant, Synapse pathology in Alzheimer's disease. *Semin. Cell Dev. Biol.* **139**, 13–23 (2023).
20. D. M. Walsh *et al.*, Naturally secreted oligomers of amyloid β protein potently inhibit hippocampal long-term potentiation in vivo. *Nature* **416**, 535–539 (2002).
21. J. J. Palop, L. Mucke, Amyloid-β–induced neuronal dysfunction in Alzheimer's disease: From synapses toward neural networks. *Nat. Neurosci.* **13**, 812–818 (2010).
22. L. A. Hulshof, D. van Nuijs, E. M. Hol, J. Middeldorp, The role of astrocytes in synapse loss in Alzheimer's disease: A systematic review. *Front. Cell. Neurosci.* **16**, 899251 (2022).
23. L. Rajendran, R. C. Paolicelli, Microglia-mediated synapse loss in Alzheimer's disease. *J. Neurosci.* **38**, 2911–2919 (2018).
24. B. Dejanovic *et al.*, Complement C1q-dependent excitatory and inhibitory synapse elimination by astrocytes and microglia in Alzheimer's disease mouse models. *Nat. Aging* **2**, 837–850 (2022).
25. S. Hong *et al.*, Complement and microglia mediate early synapse loss in Alzheimer mouse models. *Science* **352**, 712–716 (2016).
26. L. Li *et al.*, Astrocytes excessively engulf synapses in a mouse model of Alzheimer's disease. *Int. J. Mol. Sci.* **25**, 1160 (2024).
27. A. Gomez-Arboledas *et al.*, Phagocytic clearance of presynaptic dystrophies by reactive astrocytes in Alzheimer's disease. *Glia* **66**, 637–653 (2018).
28. W. S. Chung *et al.*, Astrocytes mediate synapse elimination through MEGF10 and MERTK pathways. *Nature* **504**, 394–400 (2013).
29. J.-H. Lee *et al.*, Astrocytes phagocytose adult hippocampal synapses for circuit homeostasis. *Nature* **590**, 612–617 (2021).
30. G. Lemke, C. V. Rothlin, Immunobiology of the TAM receptors. *Nat. Rev. Immunol.* **8**, 327–336 (2008).
31. T. Iram *et al.*, Megf10 is a receptor for C1Q that mediates clearance of apoptotic cells by astrocytes. *J. Neurosci.* **36**, 5185–5192 (2016).
32. H. H. Jarosz-Griffiths, E. Noble, J. V. Rushworth, N. M. Hooper, Amyloid-β receptors: The good, the bad, and the prion protein. *J. Biol. Chem.* **291**, 3174–3183 (2016).
33. T.-I. Kam, Y. Gwon, Y.-K. Jung, Amyloid beta receptors responsible for neurotoxicity and cellular defects in Alzheimer's disease. *Cell. Mol. Life Sci.* **71**, 4803–4813 (2014).
34. T. Guo *et al.*, Molecular and cellular mechanisms underlying the pathogenesis of Alzheimer's disease. *Mol. Neurodegener.* **15**, 40 (2020).
35. A. K. Y. Fu *et al.*, Blockade of EphA4 signaling ameliorates hippocampal synaptic dysfunctions in mouse models of Alzheimer's disease. *Proc. Natl. Acad. Sci. U.S.A.* **111**, 9959–9964 (2014).
36. W. Y. Fu *et al.*, Cdk5 regulates EphA4-mediated dendritic spine retraction through an ephexin1-dependent mechanism. *Nat. Neurosci.* **10**, 67–76 (2007).
37. L. M. Vargas *et al.*, EphA4 activation of c-Abl mediates synaptic loss and LTP blockade caused by amyloid-β oligomers. *PLoS One* **9**, e92309 (2014).
38. A. K. Y. Fu *et al.*, APCCdh1 mediates EphA4-dependent downregulation of AMPA receptors in homeostatic plasticity. *Nat. Neurosci.* **14**, 181–191 (2011).
39. L. Shen *et al.*, Whole genome association study of brain-wide imaging phenotypes for identifying quantitative trait loci in MCI and AD: A study of the ADNI cohort. *Neuroimage* **53**, 1051–1063 (2010).
40. Y. Goldshmit, M. P. Galea, G. Wise, P. F. Bartlett, A. M. Turnley, Axonal regeneration and lack of astrocytic gliosis in EphA4-deficient mice. *J. Neurosci.* **24**, 10064–10073 (2004).
41. Y. Goldshmit, J. Bourne, Upregulation of EphA4 on astrocytes potentially mediates astrocytic gliosis after cortical lesion in the marmoset monkey. *J. Neurotrauma* **27**, 1321–1332 (2010).
42. X. Chen *et al.*, EphA4 obstructs spinal cord neuron regeneration by promoting excessive activation of astrocytes. *Cell. Mol. Neurobiol.* **42**, 1557–1568 (2022).
43. P. T. Nguyen *et al.*, Microglial remodeling of the extracellular matrix promotes synapse plasticity. *Cell* **182**, 388–403.e15 (2020).
44. Y. Zuo, A. Lin, P. Chang, W. B. Gan, Development of long-term dendritic spine stability in diverse regions of cerebral cortex. *Neuron* **46**, 181–189 (2005).
45. S. Jin *et al.*, Inference and analysis of cell-cell communication using Cell Chat. *Nat. Commun.* **12**, 1088 (2021).
46. X.-Y. Xiong, Y. Tang, Q.-W. Yang, Metabolic changes favor the activity and heterogeneity of reactive astrocytes. *Trends Endocrinol. Metab.* **33**, 390–400 (2022).
47. P. Mulica, A. Grünewald, S. L. Pereira, Astrocyte-neuron metabolic crosstalk in neurodegeneration: A mitochondrial perspective. *Front. Endocrinol. (Lausanne).* **12**, 668517 (2021).
48. R. Afridi, J.-H. Kim, M. H. Rahman, K. Suk, Metabolic regulation of glial phenotypes: Implications in neuron-glia interactions and neurological disorders. *Front. Cell. Neurosci.* **14**, 20 (2020).
49. N. Habib *et al.*, Disease-associated astrocytes in Alzheimer's disease and aging. *Nat. Neurosci.* **23**, 701–706 (2020).
50. E. Lee *et al.*, A distinct astrocyte subtype in the aging mouse brain characterized by impaired protein homeostasis. *Nat. Aging* **2**, 726–741 (2022).
51. Z. Matusova, E. M. Hol, M. Pekny, M. Kubista, L. Valihrach, Reactive astrogliosis in the era of single-cell transcriptomics. *Front. Cell. Neurosci.* **17**, 1173200 (2023).
52. C. Escartin *et al.*, Reactive astrocyte nomenclature, definitions, and future directions. *Nat. Neurosci.* **24**, 312–325 (2021).
53. M. M. Boisvert, G. A. Erikson, M. N. Shokhirev, N. J. Allen, The aging astrocyte transcriptome from multiple regions of the mouse brain. *Cell Rep.* **22**, 269–285 (2018).
54. M. Linnerbauer, M. A. Wheeler, F. J. Quintana, Astrocyte crosstalk in CNS inflammation. *Neuron* **108**, 608–622 (2020).
55. T. Wan *et al.*, Astrocytic phagocytosis contributes to demyelination after focal cortical ischemia in mice. *Nat. Commun.* **13**, 1134 (2022).
56. R. S. Jones, A. M. Minogue, T. J. Connor, M. A. Lynch, Amyloid-β-induced astrocytic phagocytosis is mediated by CD36, CD47 and RAGE. *J. Neuroimmune Pharmacol.* **8**, 301–311 (2013).
57. M. D. Monterey, H. Wei, X. Wu, J. Q. Wu, The many faces of astrocytes in Alzheimer's disease. *Front. Neurol.* **12**, 619626 (2021).
58. S. A. Liddelow *et al.*, Neurotoxic reactive astrocytes are induced by activated microglia. *Nature* **541**, 481–487 (2017).

59. L. E. Clarke *et al.*, Normal aging induces A1-like astrocyte reactivity. *Proc. Natl. Acad. Sci. U.S.A.* **115**, E1896–E1905 (2018).
60. F. Bi *et al.*, Reactive astrocytes secrete lcn2 to promote neuron death. *Proc. Natl. Acad. Sci. U.S.A.* **110**, 4069–4074 (2013).
61. S. Mylvaganam, S. A. Freeman, S. Grinstein, The cytoskeleton in phagocytosis and macropinocytosis. *Curr. Biol.* **31**, R619–R632 (2021).
62. F. Benavente *et al.*, Novel C1q receptor-mediated signaling controls neural stem cell behavior and neurorepair. *Elife* **9**, e55732 (2020).
63. A. Sekar *et al.*, Schizophrenia risk from complex variation of complement component 4. *Nature* **530**, 177–183 (2016).
64. J. Presumey, A. R. Bialas, M. C. Carroll, Complement system in neural synapse elimination in development and disease. *Adv. Immunol.* **135**, 53–79 (2017).
65. B. Stevens *et al.*, The classical complement cascade mediates CNS synapse elimination. *Cell* **131**, 1164–1178 (2007).
66. T. Y. Huang *et al.*, SORLA attenuates EphA4 signaling and amyloid β–induced neurodegeneration. *J. Exp. Med.* **214**, 3669–3685 (2017).
67. J. Park, W.-S. Chung, Astrocyte-dependent circuit remodeling by synapse phagocytosis. *Curr. Opin. Neurobiol.* **81**, 102732 (2023).
68. E. B. Pasquale, Eph-ephrin bidirectional signaling in physiology and disease. *Cell* **133**, 38–52 (2008).
69. A. Barquilla, E. B. Pasquale, Eph receptors and ephrins: Therapeutic opportunities. *Annu. Rev. Pharmacol. Toxicol.* **55**, 465–487 (2015).
70. M. I. Fonseca *et al.*, Cell-specific deletion of C1qa identifies microglia as the dominant source of C1q in mouse brain. *J. Neuroinflammation* **14**, 48 (2017).
71. A. Litvinchuk *et al.*, Complement C3aR inactivation attenuates tau pathology and reverses an immune network deregulated in tauopathy models and Alzheimer's disease. *Neuron* **100**, 1337–1353.e5 (2018).
72. D. Toral-Rios *et al.*, Activation of STAT3 regulates reactive astrogliosis and neuronal death induced by AβO neurotoxicity. *Int. J. Mol. Sci.* **21**, 7458 (2020).
73. N. Reichenbach *et al.*, Inhibition of Stat3-mediated astrogliosis ameliorates pathology in an Alzheimer's disease model. *EMBO Mol. Med.* **11**, 1–16 (2019).
74. J. E. Herrmann *et al.*, STAT3 is a critical regulator of astrogliosis and scar formation after spinal cord injury. *J. Neurosci.* **28**, 7231–7243 (2008).
75. K. Ceyzériat, L. Abjean, M.-A. Carrillo-de Sauvage, L. Ben Haim, C. Escartin, The complex STATes of astrocyte reactivity: How are they controlled by the JAK–STAT3 pathway? *Neuroscience* **330**, 205–218 (2016).
76. G. Zhu *et al.*, Crosstalk between the oxidative stress and glia cells after stroke: From mechanism to therapies. *Front. Immunol.* **13**, 1–16 (2022).
77. S. A. Liddelow, B. A. Barres, Reactive astrocytes: Production, function, and therapeutic potential. *Immunity* **46**, 957–967 (2017), 10.1016/j.immuni.2017.06.006.
78. T. B. Puschmann, A. M. Turnley, Eph receptor tyrosine kinases regulate astrocyte cytoskeletal rearrangement and focal adhesion formation. *J. Neurochem.* **113**, 881–894 (2010).
79. J. S. Park *et al.*, Blocking microglial activation of reactive astrocytes is neuroprotective in models of Alzheimer's disease. *Acta Neuropathol. Commun.* **9**, 78 (2021).
80. Y. Wu, U. L. M. Eisel, Microglia-astrocyte communication in Alzheimer's disease. *J. Alzheimer's Dis.* **95**, 785–803 (2023).
81. S. F. Lau, H. Cao, A. K. Y. Fu, N. Y. Ip, Single-nucleus transcriptome analysis reveals dysregulation of angiogenic endothelial cells and neuroprotective glia in Alzheimer's disease. *Proc. Natl. Acad. Sci. U.S.A.* **117**, 25800–25809 (2020).
82. E. Coudert *et al.*, Annotation of biologically relevant ligands in UniProtKB using ChEBI. *Bioinformatics* **39**, btac793 (2023).
83. F. Yu, S. E. Haynes, A. I. Nesvizhskii, IonQuant enables accurate and sensitive label-free quantification with FDR-controlled match-between-runs. *Mol. Cell. Proteomics* **20**, 100077 (2021).
84. F. Yu *et al.*, Fast quantitative analysis of timsTOF PASEF data with MSFragger and IonQuant. *Mol. Cell. Proteomics* **19**, 1575–1585 (2020).
85. A. T. Kong, F. V. Leprevost, D. M. Avtonomov, D. Mellacheruvu, A. I. Nesvizhskii, MSFragger: Ultrafast and comprehensive peptide identification in mass spectrometry–based proteomics. *Nat. Methods* **14**, 513–520 (2017).
86. F. Koopmans *et al.*, SynGO: An evidence-based, expert-curated knowledge base for the synapse. *Neuron* **103**, 217–234.e4 (2019).
87. Y. Perez-Riverol *et al.*, The PRIDE database resources in 2022: A hub for mass spectrometry-based proteomics evidences. *Nucleic Acids Res.* **50**, D543–D552 (2022).